Supplementary Material

Identification and characterisation of individual nanoplastics by scanning transmission X-ray microscopy (STXM)

Alexandra Foetisch[a], Montserrat Filella[b], Benjamin Watts[c], Laure-Hélène Vinot[a], Moritz Bigalke[a*]

[a] Institute of Geography, University of Bern, Hallerstrasse 12, 3012 Bern, Switzerland

[b] Department F.-A. Forel, University of Geneva, Boulevard Carl-Vogt 66, CH-1205 Geneva, Switzerland

[c] Paul Scherrer Institute, Forschungsstrasse 111, CH-5232 Villigen-PSI, Switzerland

[*]Correspondence to: moritz.bigalke@giub.unibe.ch

Preparation of nanomaterials

Most polymer pellets were pre-grinded with a Pulverisette 11 (Fritsch, Germany). The resulting powders were successively sieved to obtain size fractions <500, <250, <100 and <63 µm. The smaller size fractions of each polymer were used to fill up a third of the MM400 grinding jar volume. In Table S1, the size fraction used corresponds to the highest size fraction added to the jars. When a pre grinding step with Pulveristte 11 was not possible, pellets were directly used for cryogrinding.

The method of nanoparticle (NP) preparation depends strongly on the initial polymer properties, the amount of plastic in the smaller fractions, the cryogrinding efficiency and the volume of ethanol used to suspend the final powder, the concentration and size distribution of NP in suspension vary depending on the polymer.

NP powders were either suspended in ethanol (pure solutions) or used as powder for the spiking experiment (except for PET (SI 5)). As suspensions were freshly prepared before each sample deposition to prevent NP aggregation or aging, the exact concentration and size distributions of the solutions used in this study are unknown.

Detailed protocol for PET nanoparticle production

Small pieces cut from a PET bottle were dissolved in 10 mL 90% tetrafluoroacetic acid (TFA) and precipitated by lowering the TFA concentration down to 20% according to Rodríguez-Hernández et al. (2019). The solution was then centrifuged at 2500 g for 30 minutes and the supernatant discarded. Instead of suspending the resulting pellet into an 0.5% sodium dodecyl sulphate (SDS) solution, as described in the original procedure, the pellet was suspended in 100 mL of 100% ethanol. The solution was allowed to settle for 1 hour in a 100 mL cylinder and the upper 50 mL collected.

Radiation damage in SEM

We observed that, in the case of PET and PA, the electron beam of the SEM induced radiation damages to the particle chemical structure when high magnification pictures were acquired (Figure S2). For PET, damage included loss of all peaks except at 285.2 eV. In the case of PA, there was a loss of the main peak at 288.2 eV and two new peaks appeared at 285 and 286.7 eV. The changes in NEXAFS spectra observed here are similar, but more extreme, than the modifications observed in another study where PET and PA films were exposed to 2700 and 1400 eV/nm^3 of soft X-ray radiation, respectively (Coffey et al., 2002). Since radiation damage depends on the dose (Egerton et al., 2004), these results show that the dose required to capture images of 20-60x10^3 x magnification with SEM is too high and induces molecular structure changes in the polymer that later prevents the NEXAFS identification of the polymer. Other polymers have also been shown to be affected by electron beam radiation (Egerton et al., 2004; Leijten et al., 2017). Therefore, we strongly recommend not to use SEM/TEM prior to STXM analyses. On the other hand, it is possible to perform imaging and spectral analysis by STXM and then analyze the sample afterwards by SEM if a high-resolution image and more precise size measurements are needed.

Radiation damage in STXM

Table S3 lists the calculated radiation dose and associated scan parameters for each STXM measurement shown in the article. The calculated dose is based simply on estimation of the irradiated sample volume and the number of absorbed photons (i.e. the photon counts from pixels beside the particle minus the counts transmitted through it). If the irradiated spot is calculated to be larger than the pixel size, then neighbouring pixels are assumed to contribute dose to each other symmetrically, which is mathematically equivalent to the same photons being restricted within the pixel boundaries. Note that the STXM instrument that performed the measurements uses a synchrotron bend-magnet source and so can be expected to have about 100 times lower photon flux than an undulator-based instrument and hence require

correspondingly longer counting times to achieve similar counting statistics and radiation dose. Further, many synchrotron beamlines suffer from carbon contamination of the optical surfaces and so the available photon flux at the carbon K-edge can vary enormously. Therefore, it can be difficult to make simple comparisons of scan parameters and the resulting radiation dose between different instruments.

The radiation dose calculations assume 100% detector efficiency, which is unlikely to be true, and the actual efficiency has not been measured. Coffey et al. (2002) assumed a detector efficiency of 30% for their radiation dose calculations. Figure S6 illustrated how the radiation dose accumulates during the measurements listed in Table S3. The steep section of the curves corresponds to the spectral region measured with a narrow photon energy steps and the vertical black lines indicate the approximate position of the C1s $\rightarrow \pi^*_{C=C}$ (e.g. phenyl and vinyl groups) and C1s $\rightarrow \pi^*_{C=O}$ (e.g. carbonyl groups) resonances. This means that the identifying spectral features are recorded with about 40% of the total radiation dose. This factor probably cancels the detector inefficiency issue to a large degree such that the dose values listed in Table S3 are realistic.

Studying the scan parameters in Table S3 shows that the analog scanning along each row of pixels (also known as “constant velocity” or “line at once” mode) does an excellent job of spreading the radiation dose evenly through the sample material in the horizontal direction. However, many scans were performed along a single row of pixels, or with the scan rows spaced further apart than the effective spot size (which combines the actual spot size with the positioning stability) and thus spreading the dose very unevenly in the vertical direction. Better choice of vertical step size could have allowed more material to be included in the measurement and correspondingly allowed other parameters to be relaxed (e.g. count time) and reduced the radiation dose required to achieve the desired measurement quality.

A common strategy to reduce radiation dose is to measure with a defocused beam. This is not a good strategy for nanoparticle measurements because it provides less control over the dose

apportionment than scanning the focused beam across the same area with the same total count time (unless the instruments scanning capabilities are not sufficient). Further, a measurement in which part of the beam passes through the sample and another part does not will give a distorted spectrum and therefore defocused measurements of nanoparticles must discard a greater region of the measured pixels close to the edge of the particle.

Particle high resolution picture and measurement

When a particle is found with STXM, its position is recorded to allow to finding it again with SEM and take a high quality picture. This picture is opened with ImageJ, the free hand selection tool is used to draw a line around the particle and the size is then measured with the “analyze particle” tool. The area, standard deviation, perimeter, circularity, Feret diameter and minimum Feret diameter are recorded for each particle (Figure S3).

When a SEM picture was not available, the size measurement was performed directly on the STXM picture.

Table S1: Details of grinding processes for each polymer.

	Pulveristte pregrinding	Size fraction used [µm]	Stainless steel beads [mm]	MM400 cryogrinding time [min]
PP	no	Pellets	3	195
PEHD	yes	<250	3	195
PELD	no	Pellets	15	195
PA	yes	<250	3	210
PMMA	yes	<63	No cryogrinding	No cryogrinding
PC	yes	<250	3	190
PVC	no	<500	15	133

Table S2: Polymer properties used to compute attenuation length of the different polymers at 320 eV. The data were collected from https://henke.lbl.gov/optical_constants/atten2.html .

Polymer	Chemical formula	Density [g/cm^3]	Attenuation length [nm]
Polypropylene	C_3H_6	0.90	328
Polyethylene	C_2H_4	0.95	309
Polyvinyl chloride	C_2H_3Cl	1.38	192
Polyethylene terephthalate	$C_{10}H_8O_4$	1.38	276
Polystyrene	C_8H_8	1.05	259
Polyamide	$C_{12}H_{22}N_2O_2$	1.14	334
Polycarbonate	$C_{16}H_{14}O_3$	1.20	272
Polymethylmetacrylate	$C_5H_8O_2$	1.19	336

Table S3: STXM scan parameters and the corresponding radiation dose estimates.

Fig	Scan File Name	Line Mode	Spot (nm)	Step (nm)	Stability [X,Y] (nm)	Effective Size [X,Y] (nm)	Dwell (ms)	Material	Dose (eV/nm^3)	Dose (MGy)
1	Sample_Stack_2020-11-27_047.hdf5	analog	40.8	100	[69.7,11.4]	[100.0,42.4]	20	PMMA	30.7	4.1
1	Sample_Stack_2020-11-27_047.hdf5	analog	40.8	100	[69.7,11.4]	[100.0,42.4]	20	PC	37.9	5.1
2	Sample_Line_2020-07-01_114.hdf5	analog	40.2	20	[15.5,8.9]	[20.0,41.1]	50	PP	464.6	82.7
2	Sample_Line_2020-07-01_083.hdf5	analog	40.2	20	[15.0,7.3]	[20.0,40.8]	20	PP	243.6	43.4
2	Sample_Line_2020-07-01_092.hdf5	analog	40.2	25	[18.4,8.3]	[25.0,41.0]	30	PP	349.4	62.2
2	Sample_Line_2020-07-01_238.hdf5	analog	40.2	30	[21.2,7.8]	[30.0,40.9]	50	PE	232.4	39.2
2	Sample_Line_2020-06-29_299.hdf5	analog	40.2	20	[15.8,7.2]	[20.0,40.8]	20	PE	223.5	37.7
2	Sample_Line_2020-06-29_320.hdf5	analog	40.2	10	[10.5,7.2]	[10.0,40.8]	20	PE	622.3	104.9
Ref	Sample_Line_2019-03-20_086.hdf5	analog	72.1	200	[137.2,7.5]	[200.0,72.5]	20	PVC	429.9	49.9
2	Sample_Line_2020-07-02_001.hdf5	analog	40.2	37.5	[26.7,7.6]	[37.5,40.9]	50	PVC	425.9	49.4
2	Sample_Line_2020-07-02_019.hdf5	analog	40.2	30	[21.9,8.1]	[30.0,41.0]	50	PVC	523.6	60.8
2	Sample_Line_2020-07-02_015.hdf5	analog	40.2	20	[15.5,8.0]	[20.0,41.0]	50	PVC	1136.4	131.9
2	Sample_Line_2020-07-01_009.hdf5	analog	40.2	25	[18.3,7.1]	[25.0,40.8]	20	PET	176	20.4
2	Sample_Line_2020-07-01_008.hdf5	analog	40.2	20	[15.1,7.1]	[20.0,40.8]	20	PET	246.8	28.7
2	Sample_Line_2020-07-01_006.hdf5	analog	40.2	12.5	[10.7,7.3]	[12.5,40.8]	20	PET	396	46
2	Sample_Line_2019-04-13_106.hdf5	analog	41	37.5	[26.8,8.5]	[37.5,44.6]	20	PS	440.5	67.2
2	Sample_Line_2019-04-13_136.hdf5	analog	41	12.5	[11.8,9.6]	[12.5,44.8]	20	PS	1933.2	295
2	Sample_Line_2020-07-02_093.hdf5	point	40.2	7.5	[9.1,9.8]	[7.5,41.4]	50	PS	1572.2	239.9
2	Sample_Line_2020-07-02_195.hdf5	point	40.2	50	[49.1,7.5]	[50.0,40.9]	50	PA	173.9	24.4
2	Sample_Line_2020-07-03_023.hdf5	point	40.2	30	[29.5,7.5]	[30.0,40.9]	50	PA	246.9	34.7
2	Sample_Line_2020-07-03_003.hdf5	point	40.2	20	[20.6,7.4]	[20.0,40.8]	50	PA	434	61
2	Sample_Line_2020-02-19_135.hdf5	analog	40.2	13	[13.8,9.5]	[13.0,41.3]	20	PC	698.3	93.2
2	Sample_Line_2020-07-02_154.hdf5	point	40.2	20	[15.9,10.7]	[20.0,41.6]	100	PC	768.6	102.6
2	Sample_Line_2020-07-02_156.hdf5	point	40.2	15	[15.6,9.6]	[15.0,41.3]	50	PC	615.7	82.2
2	Sample_Line_2020-07-03_073.hdf5	point	40.2	30	[30.5,9.1]	[30.0,41.2]	50	PMMA	479.7	64.6
2	Sample_Line_2020-07-03_089.hdf5	point	40.2	50	[35.2,9.7]	[50.0,41.3]	80	PMMA	394.3	53.1
2	Sample_Line_2020-07-03_076.hdf5	point	40.2	20	[21.2,8.6]	[20.0,41.1]	50	PMMA	863.8	116.3
2	Sample_Stack_2020-12-01_020.hdf5	analog	40.8	100	[68.9,9.7]	[100.0,41.9]	20	tea	21.8	2.9
2	Sample_Stack_2020-11-30_078.hdf5	analog	40.8	100	[69.4,11.0]	[100.0,42.3]	20	tea	25.3	3.4
2	Sample_Stack_2020-12-01_013.hdf5	analog	40.8	100	[69.5,9.9]	[100.0,42.0]	20	tea	40.5	5.5
2	Sample_Stack_2020-09-03_040.hdf5	analog	57.1	75	[51.7,6.2]	[75.0,57.5]	20	soil	23.8	3.2
2	Sample_Line_2020-09-04_184.hdf5	analog	56.2	10	[9.9,6.7]	[10.0,56.6]	20	soil	330.7	44.5
2	Sample_Stack_2020-09-02_027.hdf5	analog	57.1	133.3	[243.9,59.3]	[133.3,82.3]	20	soil	8.8	1.2
3	Sample_Stack_2020-11-27_056.hdf5	analog	40.8	100	[68.6,10.8]	[100.0,42.2]	20	PMMA	28	3.8
3	Sample_Stack_2020-11-27_097.hdf5	analog	40.8	100	[68.8,11.7]	[100.0,42.5]	80	PC	131.8	17.6
3	Sample_Stack_2020-11-27_054.hdf5	analog	40.8	100	[68.6,11.9]	[100.0,42.5]	20	PET	43.3	5
3	Sample_Stack_2020-11-30_030.hdf5	analog	40.8	100	[68.5,12.5]	[100.0,42.7]	80	PA	133.2	18.7
3	Sample_Stack_2020-09-03_023.hdf5	analog	57.1	133.3	[156.7,23.0]	[133.3,61.6]	20	PA	16.7	2.3
3	Sample_Line_2019-06-27_185.hdf5	analog	44.7	4	[8.1,10.6]	[4.0,45.9]	20	PS	8571.1	1307.8
3	Sample_Line_2019-06-27_185.hdf5	analog	44.7	4	[8.1,10.6]	[4.0,45.9]	20	PA	6646.4	934.1
4	Sample_Line_2020-09-05_009.hdf5	analog	56.2	8	[8.8,6.2]	[8.0,56.6]	20	PS	294.1	44.9
4	Sample_Line_2019-09-01_188.hdf5	analog	40.2	50	[34.9,11.8]	[50.0,44.4]	20	PS	254.8	38.9
4	Sample_Stack_2020-09-05_027.hdf5	analog	57.1	100	[69.4,6.4]	[100.0,57.5]	20	PP	11.9	2.1
4	Sample_Stack_2020-09-04_099.hdf5	analog	57.1	66.7	[45.9,6.3]	[66.7,57.5]	20	PP	22.7	4
4	Sample_Stack_2020-09-04_003.hdf5	analog	57.1	100	[68.5,5.8]	[100.0,57.4]	20	PA	21.6	3
4	Sample_Line_2019-03-21_056.hdf5	analog	44.7	30	[21.8,7.6]	[30.0,45.3]	20	PA	1208.5	169.8
4	Sample_Line_2020-09-04_210.hdf5	analog	56.2	12	[10.7,6.2]	[12.0,56.6]	20	PVC	506.7	58.8

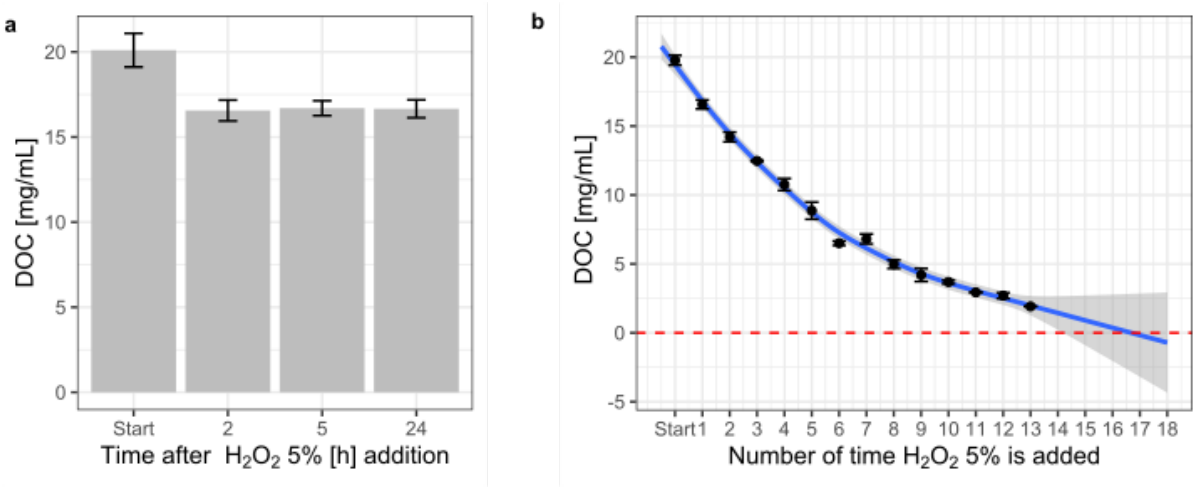

Figure S1: Effect of the H_2O_2 treatment on the dissolved organic carbon fraction (DOC) in the samples. a) If the H_2O_2 concentration is set once to 5%, the DOC decreases within the first 2 h but stays constant after up to 24 h, b) If H_2O_2 is adjusted every 2 h to 5%, the DOC concentration decreases further. The general additive model of the data is represented in with a blue line with a 95% confidence interval in grey. The measurements were acquired on triplicates; the error bars show the standard deviation.

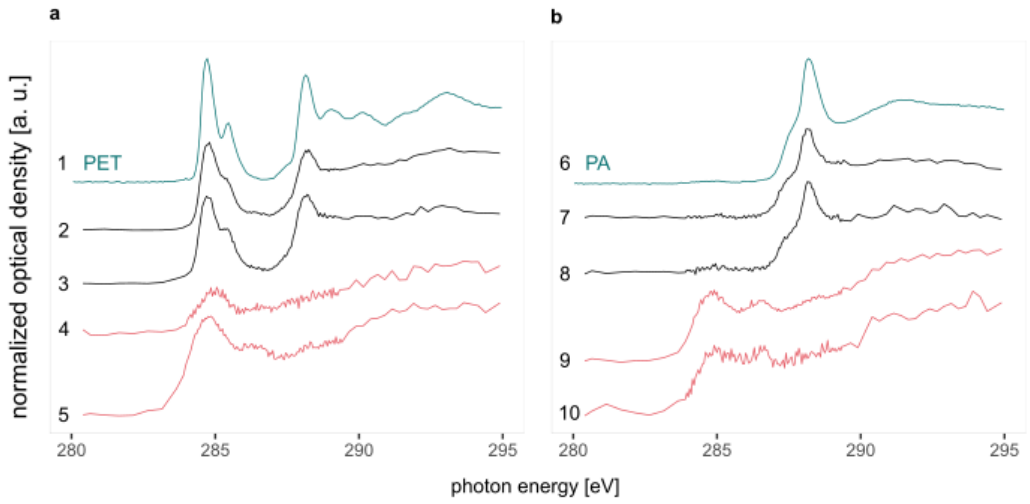

Figure S2: Illustration of the effect of SEM beam radiation on the NEXAFS of PET (a) and PA (b) nanoparticles. The reference spectra(Dhez et al., 2003) of PET and PA are the blue lines at the top of each subsection. The black spectra in position 2-3 for PET and 7-8 for PA correspond to particles for which no high magnification picture was acquired with SEM. The red spectra in position 4-5 for PET and 9-10 for PA correspond to particles for which we acquired a high magnification picture with SEM.

a

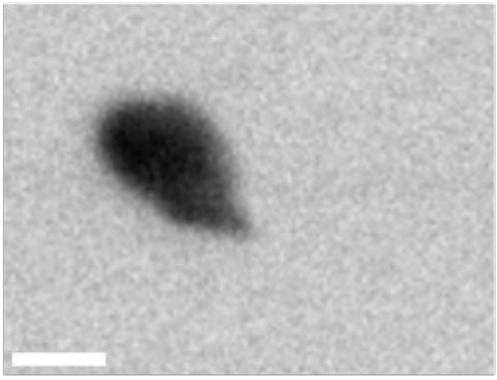

b

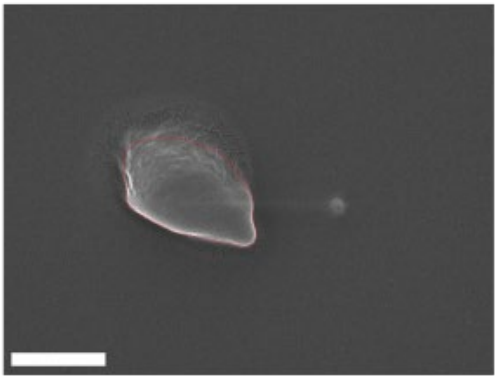

c

Area [nm]	Perimeter [nm]	Circularity [nm]	Feret [nm]	MinFeret[nm]
293	2120	821	828	476

Figure S3: Example of a particle size measurement with ImageJ. (a) STXM picture of a particle. (b) SEM picture of the same particle as in a. (c) Results of the size measurement of the particle with ImageJ. The scale bar represents 250 nm.

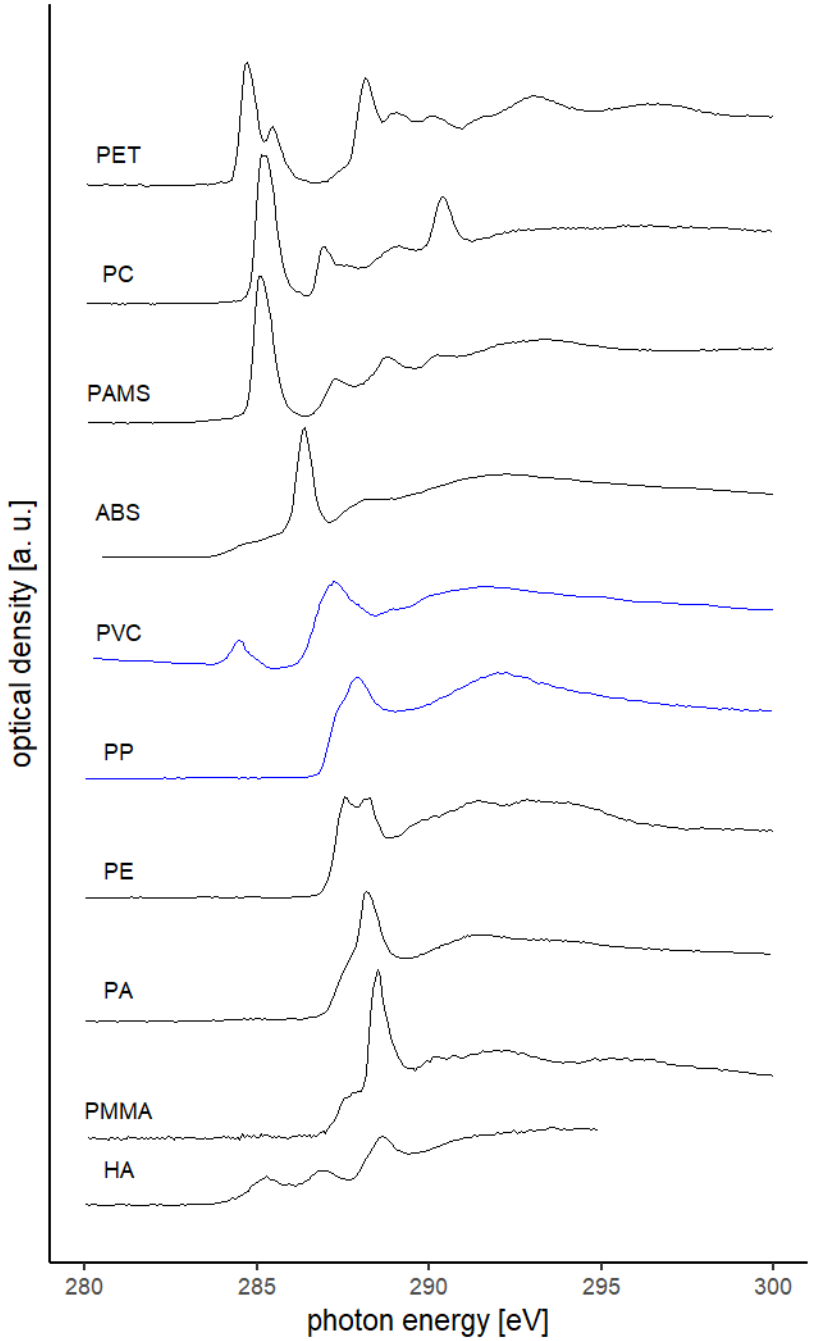

Figure S4: NEXAFS spectra of the most common polymers used as reference in this study and of humic acid as an example for natural organic substances in the environment. Except for ABS and PVC (blue lines) that were acquired for this study, all spectra come from the literature (Christl and Kretzschmar, 2007; Dhez et al., 2003). Spectra were normalized to fit the same scale.

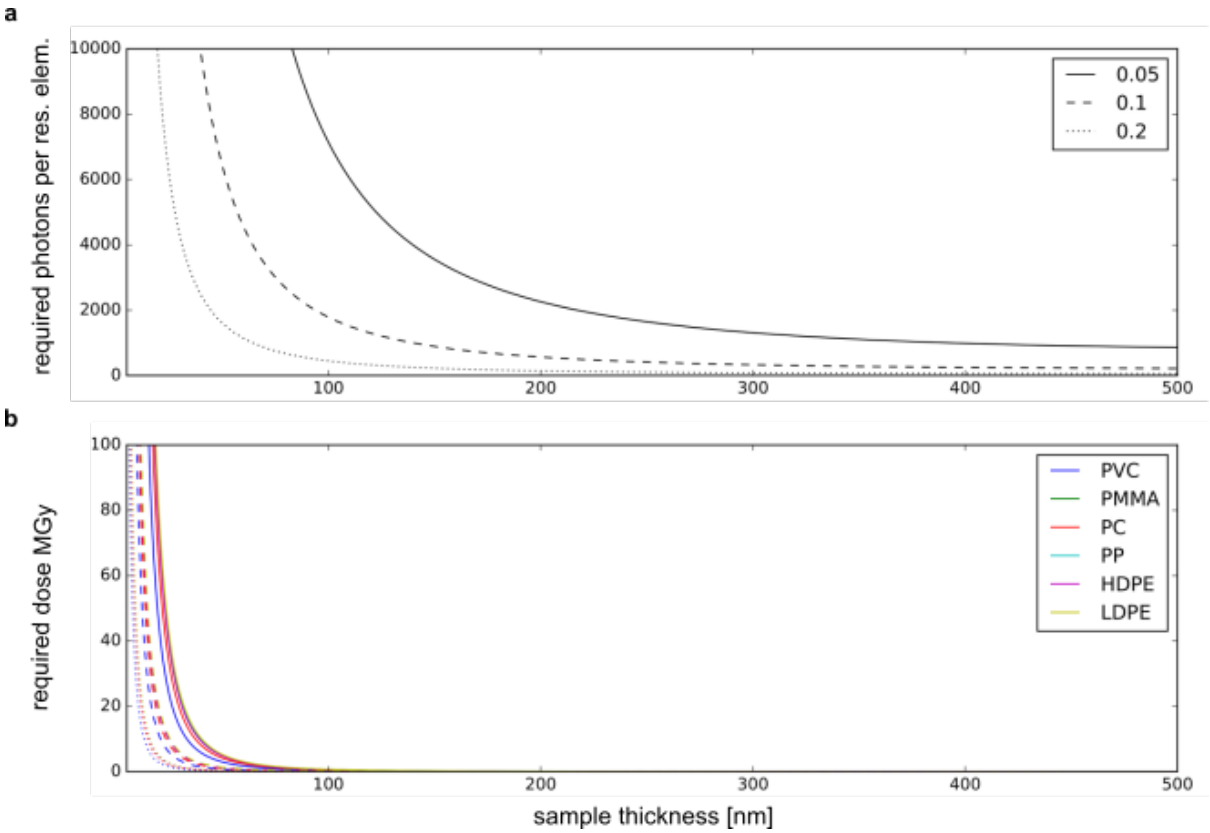

Figure S5: Theoretical limitations of STXM for nanoplastic identification. (a) Required photons per resolution element for a given spectral quality (noise fraction) as a function of the sample thickness. (b) Required dose to be applied to a given polymer as a function of the sample thickness.

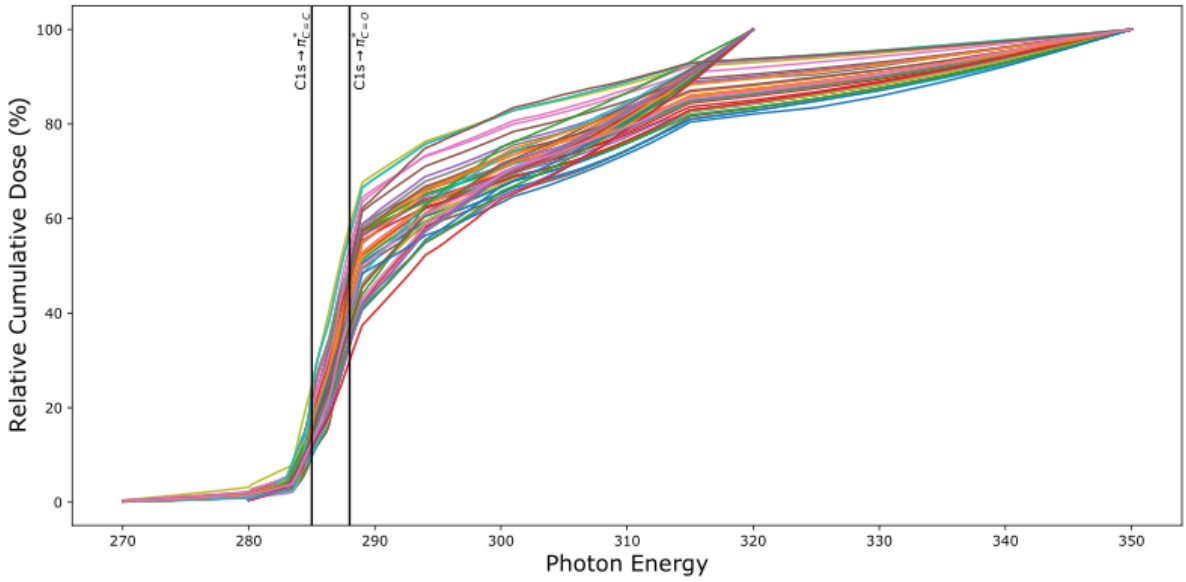

Figure S6: Relative radiation dose accumulation during the measurement of the scans listed in Table S3. The vertical black lines indicate the approximate position of the C1s → $\pi^*_{C=C}$ (e.g. phenyl and vinyl groups) and C1s → $\pi^*_{C=O}$ (e.g. carbonyl groups) resonances. This means that the identifying spectral features are recorded with about 40% of the total radiation dose listed in Table S3.

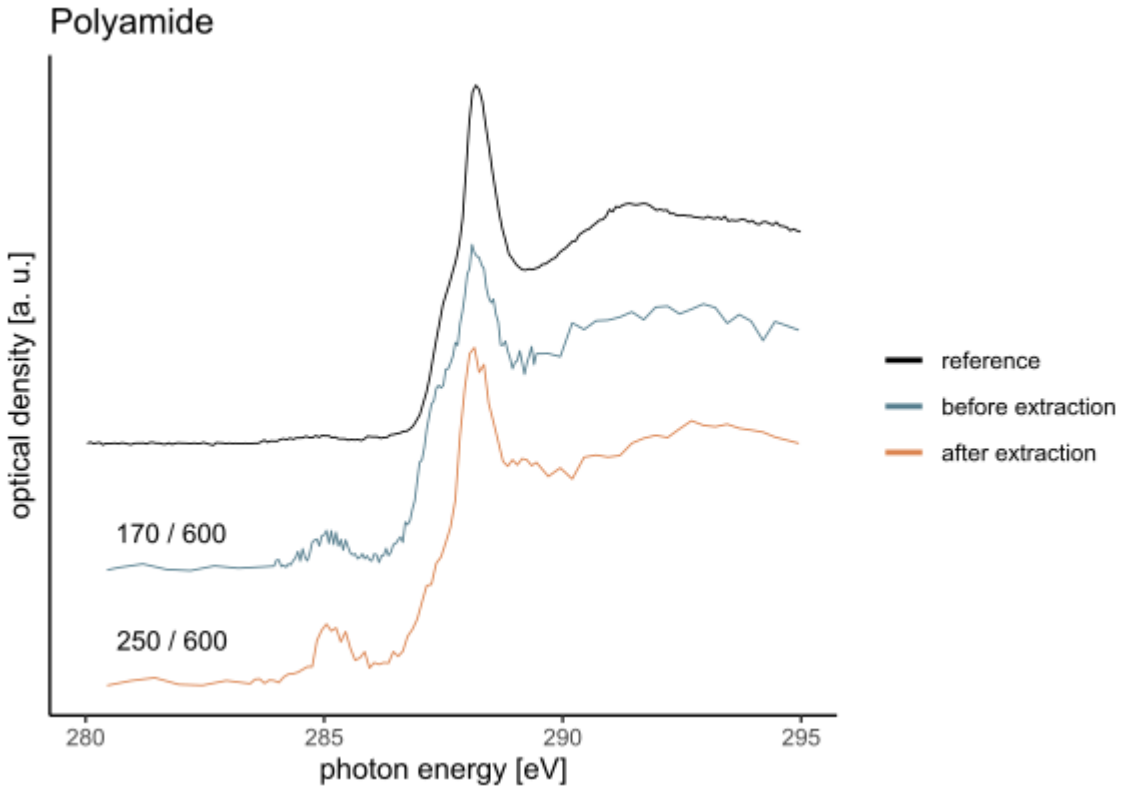

Figure S7: Spectrum quality assessment. PA reference spectrum (Dhez et al., 2003) (black line). Spectrum of a particle of PA suspended in 100% ethanol and centrifuged down a Si_2N_4 window (blue line). Spectrum of a particle after the extraction process (orange line). All spectra were normalized to fit the same scale. The thickness [nm]/ Feret diameter [nm] is given on the left side of the two measurements.

References

Christl, I., Kretzschmar, R., 2007. C-1s NEXAFS spectroscopy reveals chemical fractionation of humic acid by cation-induced coagulation. Environ. Sci. Technol. 41, 1915–1920. doi:10.1021/es062141s

Coffey, T., Urquhart, S.G., Ade, H., 2002. Characterization of the effects of soft X-ray irradiation on polymers. J. Electron Spectrosc. Relat. Phenom. 122, 65–78. doi:10.1016/S0368-2048(01)00342-5

Dhez, O., Ade, H., Urquhart, S.G., 2003. Calibrated NEXAFS spectra of some common polymers. J. Electron Spectrosc. Relat. Phenom. 128, 85–96. doi:10.1016/S0368-2048(02)00237-2

Egerton, R.F., 2009. Electron energy-loss spectroscopy in the TEM. Rep. Prog. Phys. 72, 016502. doi:10.1088/0034-4885/72/1/016502

Leijten, Z.J.W.A., Keizer, A.D.A., de With, G., Friedrich, H., 2017. Quantitative analysis of electron beam damage in organic thin films. J. Phys. Chem. C 121, 19, 10552–10561. doi:10.1021/acs.jpcc.7b01749

Rodríguez-Hernández, A.G., Muñoz-Tabares, J.A., Aguilar-Guzmán, J.C., Vazquez-Duhalt, R., 2019. A novel and simple method for polyethylene terephthalate (PET) nanoparticle production. Environ. Sci. Nano 6, 2031–2036. doi:10.1039/C9EN00365G